

# Quantum Causality: Resolving Simpson’s Paradox with $\mathcal{DO}$ -Calculus

Pilsung Kang

**Abstract**—Distinguishing correlation from causation is a fundamental challenge in machine intelligence, often representing a critical barrier to building robust and trustworthy systems. While Pearl’s  $\mathcal{DO}$ -calculus provides a rigorous framework for causal inference, a parallel challenge lies in its physical implementation. Here, we apply and experimentally validate a quantum algorithmic framework for performing causal interventions. Our approach maps causal networks onto quantum circuits where probabilistic links are encoded by controlled-rotation gates, and interventions are realized by a structural remodeling of the circuit—a physical analogue to Pearl’s “graph surgery”. We demonstrate the method’s efficacy by resolving Simpson’s Paradox in a 3-qubit model, and show its scalability by quantifying confounding bias in a 10-qubit healthcare simulation. Critically, we provide a proof-of-principle experimental validation on an IonQ Aria quantum computer, successfully reproducing the paradox and its resolution in the presence of real-world noise. This work establishes a practical pathway for quantum causal inference, offering a new computational tool to address deep-rooted challenges in algorithmic fairness and explainable AI (XAI).

**Index Terms**—Causal Inference, Quantum Computing, Simpson’s Paradox, Quantum Machine Learning,  $\mathcal{DO}$ -Calculus, Quantum Algorithms, Explainable AI (XAI), Algorithmic Fairness.

## I. INTRODUCTION

The remarkable success of modern artificial intelligence (AI) is largely built upon the ability of machine learning models to discern complex patterns and correlations from vast datasets. However, a fundamental limitation of these predominantly data-driven approaches is their inherent inability to distinguish mere correlation from true causation [1]. This distinction is not merely academic; in high-stakes domains such as medical diagnostics, financial modeling, and autonomous systems, decisions based on spurious correlations can lead to unsafe, biased, and unreliable outcomes [2]. Consequently, moving beyond pattern recognition to build models that can reason about cause and effect is a central and pressing challenge for developing the next generation of robust, fair, and trustworthy AI systems.

A stark illustration of this challenge is Simpson’s Paradox [3], a statistical phenomenon where a trend observed across an entire population reverses within its constituent subgroups once the data is partitioned. This phenomenon is particularly pernicious in the causal analysis of observational data, for example, when evaluating the efficacy of a medical *treatment* on a patient’s *outcome*. In such scenarios, the

paradox emerges when a hidden confounding variable—such as patient demographics that act as a common cause of both the treatment decision and the health outcome—is unevenly distributed across the subgroups. A machine learning model trained on such aggregated data without knowledge of the underlying causal structure would learn the spurious, reversed correlation, leading to fundamentally flawed conclusions. This presents a critical challenge for explainable AI (XAI); if a model’s recommendations, such as in clinical decision support, can be directly contradicted by a more granular analysis of the data, the model’s reliability and trustworthiness are fundamentally undermined. Therefore, resolving such paradoxes is not just a statistical exercise but a prerequisite for building AI systems whose reasoning is transparent and whose conclusions can be trusted.

The theoretical foundation for resolving such paradoxes and reasoning about causal effects is provided by Judea Pearl’s  $\mathcal{DO}$ -calculus [4]. The  $\mathcal{DO}$ -calculus offers a formal mathematical framework for computing the results of interventions, such as the interventional probability  $P(Y|\mathcal{DO}(X))$ , from observational data, provided the underlying causal graph is known. This framework serves as the gold standard for causal inference, allowing researchers to systematically distinguish true causal effects from spurious correlations. While this provides a complete logical framework, it remains a fundamentally abstract statistical procedure. A parallel line of inquiry, therefore, is whether this calculus of interventions can be directly realized within the dynamics of a physical system, offering a different paradigm for computation. Quantum computing, which operates on the principles of physical evolution, presents a natural candidate for such a physical realization, motivating the study of how the abstract “graph surgery” of the  $\mathcal{DO}$ -calculus can be mapped to concrete operations on a quantum circuit.

In prior work, we introduced a framework for quantum causal inference, establishing how quantum circuits can model causal interventions based on Pearl’s  $\mathcal{DO}$ -calculus [5]. In this paper, we apply and extend this framework to a canonical challenge in causal reasoning: Simpson’s Paradox. We validate our approach through a series of simulations and a proof-of-principle experiment on quantum hardware. First, using a 3-qubit model, we show that our method successfully resolves a classic Simpson’s Paradox scenario in a high-fidelity simulator. We then reproduce this result on an IonQ Aria trapped-ion quantum processor, confirming the viability of the approach in the presence of real-world hardware noise. Furthermore, to demonstrate scalability, we apply our framework to a complex 10-qubit causal network simulating a healthcare scenario,

Pilsung Kang is with the Department of Software Science, Dankook University, Yongin 16890, South Korea (e-mail: pilsungk@dankook.ac.kr)

successfully quantifying the confounding bias that simple statistical stratification fails to correct. Taken together, our results establish quantum causal inference as a promising computational paradigm for tackling long-standing challenges in AI fairness and XAI where complex confounding effects are prevalent. We make no claim of quantum advantage; our goal is to validate the framework on Simpson’s paradox using both simulators and quantum hardware. This v1 preprint does not release code or data; we will make all artifacts available in a subsequent arXiv version (v2).

## II. METHODOLOGY

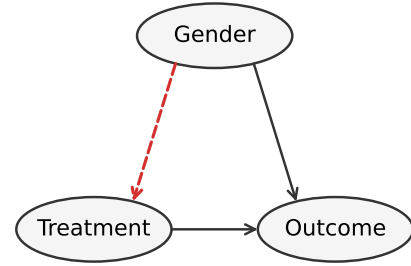
### A. Causal Framework and the DO-calculus

Simpson’s Paradox is a statistical phenomenon wherein a trend that appears in several groups of data disappears or reverses when these groups are combined. Within the framework of Pearl’s structural causal models (SCMs), this paradox is not a mathematical anomaly but a consequence of misinterpreting causal relationships from observational data. Specifically, it arises when a confounding variable influences both the treatment and the outcome, creating a spurious correlation that can obscure the true causal effect.

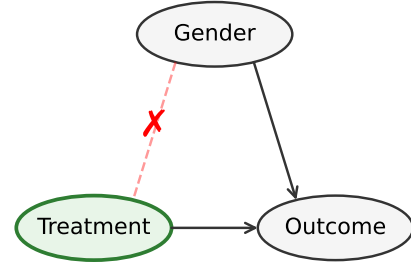
In the scenario modeled in this work, the paradox is driven by a confounder, Gender ( $G$ ), which affects both the Treatment ( $T$ ) administered and the final Outcome ( $O$ ). This causal structure can be represented by a Directed Acyclic Graph (DAG), as shown in Fig. 1a. The confounder  $G$  has a direct causal influence on both  $T$  ( $G \rightarrow T$ ) and  $O$  ( $G \rightarrow O$ ), while  $T$  also has a direct influence on  $O$  ( $T \rightarrow O$ ). The path  $G \rightarrow T$  represents the confounding bias, such as a propensity for one gender to receive a particular treatment more often than the other. To resolve the paradox, we must distinguish between two types of conditional probabilities:

- 1) **Observational Probability,  $P(O|T)$ :** This corresponds to the passive observation of “the probability of a good Outcome, given that we *see* a subject has taken the Treatment.” This probability incorporates not only the direct causal effect of  $T$  on  $O$  but also the spurious correlation created by the confounding path through  $G$ . Simpson’s Paradox manifests in this observational distribution.
- 2) **Interventional Probability,  $P(O|\mathcal{DO}(T))$ :** This corresponds to the question “what is the probability of a good Outcome *if we force* all subjects to take the Treatment?”, which is equivalent to the outcome of a randomized controlled trial (RCT). In the causal graph, the  $\mathcal{DO}(T)$  operator is realized by performing “graph surgery”: all incoming arrows to the variable  $T$  (in this case, the  $G \rightarrow T$  link) are severed, resulting in the modified causal graph shown in Fig. 1b. By blocking the confounding path,  $P(O|\mathcal{DO}(T))$  isolates the pure causal effect of  $T$  on  $O$ .

The central goal of our quantum experiment is to simulate these two distinct probability distributions. By comparing the paradoxical results from the observational distribution with the true causal effect revealed by the interventional distribution, we demonstrate a resolution to Simpson’s Paradox.



(a) Observational Causal Graph



(b) Interventional Causal Graph

Fig. 1: The causal Directed Acyclic Graphs (DAGs) for the 3-qubit Simpson’s Paradox model. (a) The observational model, where  $G$  (Gender) is a common-cause confounder for  $T$  (Treatment) and  $O$  (Outcome). (b) The interventional model for  $\mathcal{DO}(T = t)$ , where the confounding path  $G \rightarrow T$  has been surgically removed.

### B. Quantum Implementation of Causal Interventions

To translate the abstract structure of a causal DAG into a physical quantum process, we map each variable in the model to a corresponding qubit. The binary states of the variable are represented by the computational basis states of the qubit,  $|0\rangle$  and  $|1\rangle$ .

A causal arrow between two variables, for instance from a cause  $A$  to an effect  $B$  ( $A \rightarrow B$ ), is implemented using a controlled quantum gate, where the state of the qubit representing  $A$  dictates the operation applied to the qubit representing  $B$ . In this work, we primarily use the controlled  $Y$ -rotation gate,  $\text{CRY}(\theta)$ , to encode these probabilistic causal links. A  $\text{CRY}(\theta)$  gate applies a rotation around the  $Y$ -axis,  $R_Y(\theta)$ , to the target qubit ( $B$ ) if and only if the control qubit ( $A$ ) is in the state  $|1\rangle$ .

The rotation angle,  $\theta$ , serves as a tunable parameter that directly corresponds to the strength of the causal relationship. If the target qubit  $B$  starts in the state  $|0\rangle$ , the probability of it transitioning to  $|1\rangle$  under the influence of the control qubit  $A$  being in state  $|1\rangle$  is given by the conditional probability  $P(B = 1|A = 1) = \sin^2(\theta/2)$ . A larger angle  $\theta$  thus corresponds to a stronger causal influence. For cases where the causal link is conditional on the cause being 0 (e.g., in our confounding model where males,  $G=0$ , have a higher treatment probability), the control operation is wrapped with  $X$  gates on the control qubit.

By composing a series of these controlled-rotation gates according to the arrows in a given DAG, we construct a quantum

circuit that generates a final state distribution equivalent to the joint probability distribution defined by the SCMs. This allows us to construct quantum circuits that model the causal systems under study.

To model the observational distribution, we construct a quantum circuit that directly mirrors the structure of the given causal DAG. Every causal arrow in the graph is translated into a corresponding controlled-rotation gate, as described above, and these gates are composed in sequence to build the full circuit. Crucially, this includes the gates representing the confounding path—in our case, the link from the confounder (Gender) to the treatment (Treatment),  $G \rightarrow T$ . The resulting quantum circuit, which we term the *observational circuit*, is thus a physical analogue of the complete, confounded causal system. Executing this circuit and measuring the final state of the qubits yields samples from the observational joint probability distribution  $P(O, T, G)$ , which inherently contains the statistical biases induced by the confounding variable.

To sample from an interventional distribution, such as  $P(O, G | \mathcal{DO}(T = t))$ , we implement the  $\mathcal{DO}$ -operator by performing a procedure we term “circuit surgery” [5]. This process begins with the observational circuit. We then identify and physically remove all quantum gates that correspond to the causal arrows pointing *into* the variable being intervened upon. For an intervention on the Treatment variable (T), this means removing the gates that encode the confounding path  $G \rightarrow T$ . After severing these incoming causal links, the state of the intervention qubit is deterministically set to the desired value; for instance, for the intervention  $\mathcal{DO}(T = 1)$ , an X gate is applied to the treatment qubit to force its state to  $|1\rangle$ . The resulting *interventional circuit* is structurally different from the observational one and represents a new causal world where the treatment is no longer influenced by its original causes. Consequently, executing this modified circuit produces measurement outcomes that are fair samples from the post-intervention distribution  $P(O, G | \mathcal{DO}(T = t))$ , from which the true, unconfounded causal effect of the treatment can be calculated.

### C. Specific Circuit Models for Simpson’s Paradox

To validate our proposed methodology, we designed and simulated two distinct quantum circuits: a minimal 3-qubit model to clearly illustrate the core principles, and a more complex 10-qubit model to demonstrate the scalability of our approach to networks with multi-level confounding.

1) *3-Qubit Foundational Model*: This model serves as a minimal physical realization of Simpson’s Paradox using a 3-qubit system. Each qubit is assigned to a core binary variable as follows: qubit  $q_0$  represents Gender (G), where  $|0\rangle$  corresponds to ‘male’ and  $|1\rangle$  to ‘female’; qubit  $q_1$  represents Treatment (T), where  $|0\rangle$  indicates ‘untreated’ and  $|1\rangle$  indicates ‘treated’; and qubit  $q_2$  represents the Outcome (O), where  $|0\rangle$  is a ‘poor’ outcome and  $|1\rangle$  is a ‘good’ outcome. The observational circuit is constructed to embody the necessary causal structure for the paradox to emerge. First, a strong confounding link ( $G \rightarrow T$ ) is engineered such that one group (males,  $G=0$ ) has a high probability ( $\sim 85\%$ ) of receiving the

treatment, while the other (females,  $G=1$ ) has a low probability ( $\sim 15\%$ ). Second, direct causal links are implemented for the confounder-outcome relationship ( $G \rightarrow O$ , where females have a better baseline outcome) and the treatment-outcome relationship ( $T \rightarrow O$ , where the treatment is beneficial for all subjects). The detailed structures of the resulting observational and interventional circuits for this model are depicted in Fig. 2.

2) *10-Qubit Scalability Model*: To demonstrate the utility of our method on more complex, realistic problems, we developed a 10-qubit model simulating a multi-level healthcare scenario. The model features a main causal chain where demographic variables influence treatment decisions, which in turn affect a cascade of healthcare quality factors and the final patient outcome (e.g., Age  $\rightarrow$  Income  $\rightarrow \dots \rightarrow$  Treatment  $\rightarrow \dots \rightarrow$  Outcome). The circuit also includes additional confounding paths (e.g., Age  $\rightarrow$  Insurance) to create a deeply confounded system where the true causal effect of the treatment is obscured by multiple interacting variables. This model serves as a more challenging testbed to assess the ability of our quantum causal inference framework to disentangle complex causal relationships that are difficult to address with simple stratification.

## III. EXPERIMENTS AND RESULTS

### A. Experimental Setup

All experiments were designed and executed within a Python 3 environment, utilizing the Qiskit open-source framework (v1.4.3) [6] for quantum circuit construction and execution. Data analysis and visualization were performed using the standard scientific Python libraries, including Numpy [7], Scipy [8], and Matplotlib [9].

Our study involved two types of backends: a high-performance classical simulator and a physical quantum processing unit (QPU). All simulations were performed using the AerSimulator from the `qiskit_aer` package. The 3-qubit foundational model simulation was conducted over 30 trials with 15,000 shots per circuit to achieve high statistical precision. The 10-qubit scalability model was simulated for 10 trials with 15,000 shots each. The experimental validation was performed on the IonQ Aria trapped-ion quantum computer, accessed via the `qiskit-ionq` provider. The hardware experiment consisted of 3 successful trials with 1024 shots per circuit.

To ensure statistical significance, all reported 95% confidence intervals for the treatment effects are derived from the distribution of the outcomes across these independent trials. The intervals are calculated using a normal approximation, defined as the sample mean  $\pm 1.96$  times the standard error of the mean.

### B. Result 1: Simpson’s Paradox on a 3-Qubit Model: Simulation and Experimental Validation

We first demonstrate our framework on the 3-qubit foundational model, performing both an ideal noise-free simulation and an experimental validation on a quantum processor. This dual approach allows us to first establish the theoretical correctness of our method in a baseline scenario and then

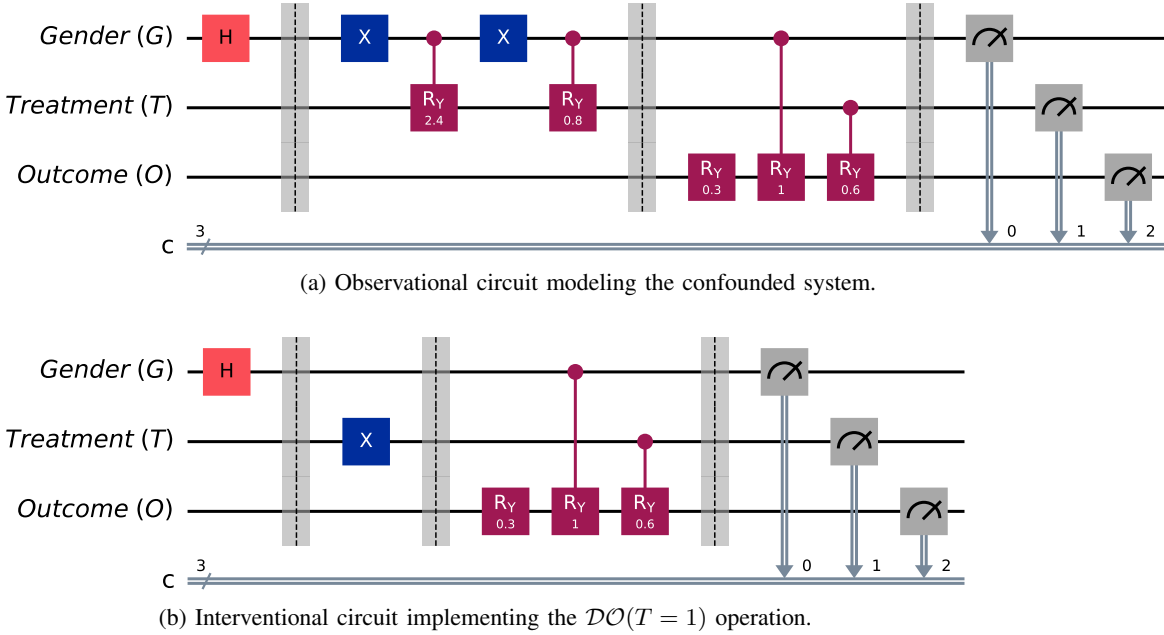


Fig. 2: Quantum circuits for the 3-qubit Simpson’s Paradox model. (a) The observational circuit encodes all causal links from the DAG in Fig. 1, including the confounding path  $G \rightarrow T$ . (b) The interventional circuit is created via “circuit surgery,” where the gates corresponding to the  $G \rightarrow T$  link are removed and the treatment qubit is deterministically set to the state  $|1\rangle$ .

TABLE I: Comparison of 3-qubit Simpson’s Paradox results from the ideal simulator and the IonQ Aria QPU ( $n=3$  trials, 1024 shots per circuit). In both the simulation and the QPU experiment, the treatment effect is positive within the male and female subgroups, but the aggregated observational effect becomes negative, demonstrating the paradox. The quantum causal intervention ( $\mathcal{DO}$ -operation) successfully resolves this paradox in both cases by revealing the true, positive causal effect. The QPU data qualitatively reproduces the simulation results, while its wider confidence intervals highlight the impact of real-world hardware noise on the statistical outcomes.

Analysis Group	Ideal Simulation		IonQ QPU	
	Effect Size ( $\Delta P$ )	95% CI	Effect Size ( $\Delta P$ )	95% CI
Observational, Male ( $G=0$ )	+0.166	[+0.163, +0.169]	+0.116	[+0.105, +0.127]
Observational, Female ( $G=1$ )	+0.296	[+0.292, +0.300]	+0.292	[+0.184, +0.400]
Observational, Overall	<b>-0.061</b>	<b>[-0.063, -0.058]</b>	<b>-0.026</b>	<b>[-0.066, +0.014]</b>
Causal, Overall ( $\mathcal{DO}$ )	+0.232	[+0.230, +0.234]	+0.222	[+0.195, +0.249]

to directly assess its practical performance and the impact of real-world hardware noise. The complete results, which directly compare the simulation and the IonQ QPU execution, are presented in Table I and Fig. 3. As we will show, the experimental results successfully reproduce the key features of the ideal simulation, confirming the viability of our approach.

In the simulation, the observational analysis reveals positive treatment effects for both male (+0.166) and female (+0.296) subgroups, which reverse to a negative overall effect of  $-0.061$ . Critically, this paradoxical structure is qualitatively reproduced on the quantum processor, which measured subgroup effects of +0.116 and +0.292 respectively, against a negative-trending overall effect of  $-0.026$ . Furthermore, the causal resolution is robustly demonstrated in both environments. The quantum causal intervention yields a true average causal effect (ACE) of +0.232 in the simulation and a consistent +0.222 on the QPU. A direct comparison highlights the impact of hardware noise; while the strong causal signal remains statistically significant in the QPU data

(95% CI [0.195, 0.249]), the confidence interval for the weaker observational overall effect,  $[-0.066, +0.014]$ , now includes zero, underscoring the challenge of observing subtle statistical phenomena on noisy hardware.

### C. Result 2: Scalability on a Complex Network (Simulation)

To assess the scalability and practical utility of our framework beyond minimal models, we applied it to a complex 10-qubit causal network simulating a multi-level healthcare scenario. As described in the Methodology section, this model was designed as a more challenging testbed, featuring a long causal chain and multiple confounding pathways that are difficult to disentangle using conventional statistical methods. The simulation results, summarized in Table II, demonstrate that while the observational data suggests a positive treatment effect, it significantly underestimates the true causal impact—a bias that our interventional method successfully quantifies.

The detailed results, presented in Table II and visualized in Fig. 4, reveal the insufficiency of conventional statistical con-

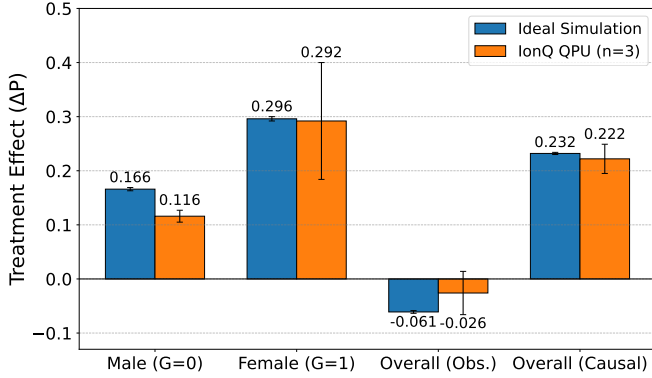


Fig. 3: Comparison of 3-qubit Simpson’s Paradox results from ideal simulation (blue bars) and the IonQ Aria QPU (orange bars). Both the simulation and the QPU experiment demonstrate the core phenomenon: the treatment effect is positive within the male and female subgroups, but reverses to become negative when aggregated (‘Overall (Obs.)’). In both cases, the quantum causal intervention ( $\mathcal{DO}$ -operation) successfully resolves the paradox by revealing a robustly positive true causal effect (‘Overall (Causal)’). The QPU results qualitatively reproduce the simulation’s trend, validating the method on real hardware, while the larger error bars on the QPU data reflect the impact of physical noise. Error bars represent 95% confidence intervals, calculated over 30 trials for the simulation and 3 successful trials for the QPU experiment.

TABLE II: Comparison of Treatment Effects under Various Analysis Levels in the 10-Qubit System. The ‘Bias’ column represents the deviation of each calculated effect from the true causal effect (+0.486) discovered via  $\mathcal{DO}$ -calculus.

Analysis Level	Effect Size ( $\Delta P$ )	95% CI	Bias
Overall Observational	+0.377	[0.371, 0.383]	-0.109
Stratified by Age	+0.497	[0.491, 0.503]	+0.011
Stratified by Region	+0.406	[0.396, 0.416]	-0.080
<b>Causal Intervention</b>	<b>+0.486</b>	<b>[0.481, 0.490]</b>	<b>0.000</b>

trols in this complex network. The overall observational data yields a treatment effect of +0.377 (95% CI [0.371, 0.383]). Attempting to correct for this by stratifying on a single confounding variable provides only a partial and inconsistent solution; stratification by the ‘Region’ variable adjusts the effect to +0.406, while stratification by the more influential ‘Age’ variable adjusts it to +0.497. In contrast, our quantum causal intervention method, which accounts for all confounding paths simultaneously, isolates the true average causal effect (ACE) to be +0.486 (95% CI [0.481, 0.490]). This demonstrates that in systems with multi-level confounding, where the choice of a single stratification variable can lead to different conclusions, our quantum  $\mathcal{DO}$ -calculus implementation provides a robust and definitive means of identifying the true causal impact.

#### IV. DISCUSSIONS

In this work, we have demonstrated a quantum algorithmic framework for causal inference, validating its ability

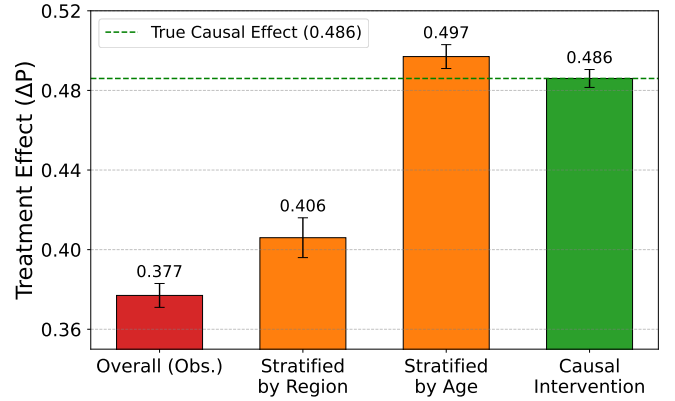


Fig. 4: Quantifying confounding bias in the 10-qubit healthcare simulation. This figure compares the treatment effect ( $\Delta P$ ) calculated from raw observational data against results from conventional stratification and our quantum causal intervention. The observational data (‘Overall (Obs.)’) significantly underestimates the true causal effect, yielding an effect of +0.377, whereas the true effect revealed by the intervention (‘Causal Intervention’) is +0.486. Simple stratification by a single variable provides only a partial and inconsistent correction; stratifying by Region yields an effect of +0.406, while stratifying by the stronger confounder, Age, yields +0.497. This demonstrates the robustness of the quantum  $\mathcal{DO}$ -calculus approach in isolating the true causal effect from complex confounding structures. The horizontal dashed line indicates the true causal effect for reference. Error bars represent 95% confidence intervals calculated over 10 trials.

to resolve statistical paradoxes and quantify confounding bias through both high-fidelity simulations and a proof-of-principle experiment on a quantum processor. Beyond the specific numerical outcomes, our findings support a deeper interpretation of quantum circuits as direct physical analogues for SCMs. As established in our foundational work [5], this framework uses superposition to represent the probabilistic nature of causal variables. Crucially, both the arrows representing true causal effects and those forming the confounding structures that induce spurious correlations are realized by the same physical mechanism: entanglement generated via controlled gates. From this perspective, the  $\mathcal{DO}$ -operator is implemented via the circuit surgery procedure—a structural modification that creates a new physical system corresponding to the interventional world. Building on this interpretation, the following sections will analyze the specific biases observed in our models, position our work relative to classical methods and its implications for AI, and discuss the limitations and future directions of this approach.

##### A. Interpretation of Confounding Bias in Causal Models

Our results provide a tale of two confounding scenarios, illustrating the different ways in which observational data can be misleading. In the 3-qubit foundational model, we observed a classic case of Simpson’s Paradox where the confounding was strong enough to completely reverse the sign of the

treatment effect. The data showed a statistically significant positive effect within subgroups, which flipped to a negative effect in the aggregated observational data (e.g., effect =  $-0.061$  in simulation). Our quantum intervention correctly identified this reversal and recovered the true, positive causal effect.

The 10-qubit model presented a more subtle, and perhaps more realistic, scenario. Here, the confounding was not strong enough to reverse the sign of the effect, but it nonetheless created a significant quantitative bias. The observational data suggested a positive treatment effect of  $+0.377$ , which is a substantial underestimation of the true causal effect of  $+0.486$  revealed by our quantum intervention. The practical implications of this latter finding are profound. A model or policy based purely on the observational data would have undervalued the treatment’s true efficacy by more than 22% ( $0.109/0.486$ ). In a real-world context, such as evaluating a new medical intervention or a public policy, an error of this magnitude could lead to the premature rejection of a beneficial treatment or the misallocation of critical resources. This highlights the critical need for computational tools that can move beyond simple correlations to robustly estimate true causal impacts, a role our quantum framework is designed to fill.

### B. Implications and Comparison with Classical Methods

The ability to perform physical causal interventions on a quantum computational substrate has significant implications across several scientific and technological domains. In machine intelligence, our framework offers a new tool for enhancing explainability (XAI) and algorithmic fairness. By moving beyond correlational models, it provides a means to probe the true causal drivers behind a model’s decisions, helping to identify and mitigate biases learned from confounded data. Beyond AI, this approach could be applied to complex network problems in fields such as systems biology, materials science, and econometrics, where simulating interventions to understand the effects of a specific gene, material property, or policy is a central challenge.

This computational approach to intervention stands in contrast to the gold standard of classical experimental design: the RCT. While RCTs achieve causal identification by physically randomizing subjects, they can be prohibitively expensive, time-consuming, unethical (e.g., forcing subjects to adopt harmful behaviors), or physically impossible (e.g., re-running historical events). Our quantum framework, acting as a “computational laboratory,” allows such interventions to be simulated efficiently on a validated causal model. This enables researchers to explore a vast range of “what-if” scenarios that are inaccessible to traditional experimental methods.

It is important to position our quantum approach relative to established classical methods for causal inference, such as covariate adjustment based on the back-door criterion or instrumental variable analysis [4]. For systems where the causal graph is known and the number of variables is small enough to be handled by classical computers, these statistical methods are both efficient and sufficient. However, the advantage of a quantum approach emerges in scenarios where

the system’s complexity becomes a prohibitive barrier for classical computation. For causal networks with a vast number of variables and highly intricate dependencies, the state space can grow exponentially, making it intractable to classically represent the joint probability distribution or sample from it. By leveraging quantum properties like superposition and entanglement, a quantum processor can potentially explore these high-dimensional causal structures more efficiently. While the current work does not demonstrate a quantum advantage, our successful experimental validation serves as a foundational proof-of-principle, establishing a pathway toward a potential “quantum advantage for causal inference” on future, fault-tolerant quantum hardware.

### C. Limitations and Future Directions

While our work establishes a viable framework for quantum causal inference, it is important to clarify its scope and current limitations. The experiments presented in this paper focus on causal effect estimation and therefore presuppose that the underlying causal graph is known a priori, which is a standard assumption for applying the  $DO$ -calculus. However, this does not mean the framework is inapplicable when the true graph is unknown. Indeed, the ability of our circuit-based approach to act as a “computational laboratory” allows it to serve as a powerful tool for causal model testing. Researchers can formulate several competing causal hypotheses, compile each into a distinct quantum circuit, and compare the simulated observational data from each circuit against real-world data to determine the most plausible causal model. While a full exploration of such a quantum-enhanced hypothesis testing workflow is beyond the scope of this paper, it represents a significant direction for future research.

Second, while we have provided a successful proof-of-principle on current quantum hardware, a significant gap remains between the performance on small-scale problems and the requirements for achieving a practical quantum advantage on large-scale problems with noisy intermediate-scale quantum (NISQ) devices.

These limitations directly highlight several exciting avenues for future research. A primary direction is the development of quantum algorithms for causal discovery, which would aim to learn the causal graph itself from quantum observational and interventional data, thereby removing our framework’s main prerequisite. Another critical research path is the design of noise-robust causal inference circuits. This could involve co-designing algorithms with specific hardware properties in mind or integrating quantum error mitigation and correction techniques to improve the fidelity of results on current and future NISQ processors. Progress in these areas will be crucial for moving quantum causal inference from a proof-of-principle, as demonstrated here, to a powerful tool for scientific discovery in complex systems.

## V. CONCLUSION

In this work, we addressed the fundamental challenge of causal inference in machine intelligence by applying and experimentally validating a quantum algorithmic framework

for implementing Pearl’s  $DO$ -calculus. By representing causal networks as quantum circuits and performing interventions via circuit surgery, our method provides a direct, physically-grounded means of distinguishing true causal effects from spurious correlations. Our framework successfully resolved Simpson’s Paradox in a 3-qubit model, demonstrated its potential to quantify bias in a complex 10-qubit simulation, and, most critically, was validated in a proof-of-principle experiment on an IonQ quantum computer. This work establishes a practical pathway for quantum causal inference, offering a new class of tools for building more robust, fair, and explainable AI systems. By bridging the mathematical rigor of causal models with the physical dynamics of quantum systems, our approach opens a new frontier for research at the intersection of quantum computing and machine intelligence.

#### ACKNOWLEDGMENTS

This work was supported by the National Research Foundation of Korea (NRF) grant funded by the Korea government (Ministry of Science and ICT (MSIT)), grant number 2020R1F1A1067619. This research was supported by ‘Quantum Information Science R&D Ecosystem Creation’ through NRF funded by the Korea government (MSIT), grant number 2020M3H3A1110365.

#### APPENDIX

##### QUANTUM GATE PARAMETERS FOR THE CAUSAL MODELS

The specific rotation angles ( $\theta$ ) for all gates used to construct the 3-qubit and 10-qubit causal models are detailed in Table III.

#### REFERENCES

- [1] J. Pearl, *Causality: Models, Reasoning and Inference*, 2nd ed. USA: Cambridge University Press, 2009.
- [2] D. Ueda, T. Kakinuma, S. Fujita, K. Kamagata, Y. Fushimi, R. Ito, Y. Matsui, T. Nozaki, T. Nakaura, N. Fujima, F. Tatsugami, M. Yanagawa, K. Hirata, A. Yamada, T. Tsuboyama, M. Kawamura, T. Fujioka, and S. Naganawa, “Fairness of artificial intelligence in healthcare: review and recommendations,” *Japanese Journal of Radiology*, vol. 42, no. 1, pp. 3–15, Jan 2024. [Online]. Available: <https://doi.org/10.1007/s11604-023-01474-3>
- [3] E. H. Simpson, “The Interpretation of Interaction in Contingency Tables,” *Journal of the Royal Statistical Society. Series B (Methodological)*, vol. 13, no. 2, pp. 238–241, 1951.
- [4] J. Pearl, “Causal Diagrams for Empirical Research,” *Biometrika*, vol. 82, no. 4, pp. 669–710, 1995.
- [5] P. Kang, “Quantum Entanglement as Super-Confounding: From Bell’s Theorem to Robust Machine Learning,” 2025. [Online]. Available: <https://arxiv.org/abs/2508.19327>
- [6] A. Javadi-Abhari, M. Treinish, K. Krsulich, C. J. Wood, J. Lishman, J. Gacon, S. Martiel, P. D. Nation, L. S. Bishop, A. W. Cross, B. R. Johnson, and J. M. Gambetta, “Quantum Computing with Qiskit,” 2024.
- [7] C. R. Harris, K. J. Millman, S. J. van der Walt, R. Gommers, P. Virtanen, D. Cournapeau, E. Wieser, J. Taylor, S. Berg, N. J. Smith, R. Kern, M. Picus, S. Hoyer, M. H. van Kerkwijk, M. Brett, A. Haldane, J. F. del Río, M. Wiebe, P. Peterson, P. Gérard-Marchant, K. Sheppard, T. Reddy, W. Weckesser, H. Abbasi, C. Gohlke, and T. E. Oliphant, “Array programming with NumPy,” *Nature*, vol. 585, no. 7825, pp. 357–362, Sep 2020.

- [8] P. Virtanen, R. Gommers, T. E. Oliphant, M. Haberland, T. Reddy, D. Cournapeau, E. Burovski, P. Peterson, W. Weckesser, J. Bright, S. J. van der Walt, M. Brett, J. Wilson, K. J. Millman, N. Mayorov, A. R. J. Nelson, E. Jones, R. Kern, E. Larson, C. J. Carey, Í. Polat, Y. Feng, E. W. Moore, J. VanderPlas, D. Laxalde, J. Perktold, R. Cimrman, I. Henriksen, E. A. Quintero, C. R. Harris, A. M. Archibald, A. H. Ribeiro, F. Pedregosa, P. van Mulbregt, A. Vijaykumar, A. P. Bardelli, A. Rothberg, A. Hilboll, A. Kloeckner, A. Scopatz, A. Lee, A. Rokem, C. N. Woods, C. Fulton, C. Masson, C. Häggström, C. Fitzgerald, D. A. Nicholson, D. R. Hagen, D. V. Pasechnik, E. Olivetti, E. Martin, E. Wieser, F. Silva, F. Lenders, F. Wilhelm, G. Young, G. A. Price, G.-L. Ingold, G. E. Allen, G. R. Lee, H. Audren, I. Probst, J. P. Dietrich, J. Silterra, J. T. Webber, J. Slavič, J. Nothman, J. Buchner, J. Kulick, J. L. Schönberger, J. V. de Miranda Cardoso, J. Reimer, J. Harrington, J. L. C. Rodríguez, J. Nunez-Iglesias, J. Kuczynski, K. Tritz, M. Thoma, M. Neville, M. Kümmerer, M. Bolingbroke, M. Tartre, M. Pak, N. J. Smith, N. Nowaczyk, N. Shebanov, O. Pavlyk, P. A. Brodtkorb, P. Lee, R. T. McGibbon, R. Feldbauer, S. Lewis, S. Tygier, S. Sievert, S. Vigna, S. Peterson, S. More, T. Pudlik, T. Oshima, T. J. Pingel, T. P. Robitaille, T. Spura, T. R. Jones, T. Cera, T. Leslie, T. Zito, T. Krauss, U. Upadhyay, Y. O. Halchenko, Y. Vázquez-Baeza, and S. 1.0 Contributors, “SciPy 1.0: fundamental algorithms for scientific computing in Python,” *Nature Methods*, vol. 17, no. 3, pp. 261–272, Mar 2020.
- [9] J. D. Hunter, “Matplotlib: A 2D Graphics Environment,” *Computing in Science & Engineering*, vol. 9, no. 3, pp. 90–95, 2007.

**Pilsung Kang** is an Associate Professor in the Department of Software Science at Dankook University, South Korea. His research interests include parallel systems, high-performance software, and quantum computing. Kang has a PhD in computer science from Virginia Tech.

TABLE III: Quantum gate parameters for the causal models. All rotation angles  $\theta$  are given in radians.

Causal Link / Base Rate	Condition	Quantum Gate	Angle ( $\theta$ )
<i>3-Qubit Foundational Model</i>			
Gender (G) Distribution	-	$H(g_0)$	-
Gender (G) $\rightarrow$ Treatment (T)	Male (G=0)	$CRY(\theta)$	2.4
	Female (G=1)	$CRY(\theta)$	0.8
Outcome (O) Base Rate	-	$R_Y(\theta)$	0.3
Gender (G) $\rightarrow$ Outcome (O)	Female (G=1)	$CRY(\theta)$	1.0
Treatment (T) $\rightarrow$ Outcome (O)	-	$CRY(\theta)$	0.6
<i>10-Qubit Scalability Model</i>			
Age (A) Base Rate	-	$R_Y(\theta)$	1.0
Age (A) $\rightarrow$ Income (I)	Old (A=1)	$CRY(\theta)$	0.8
Income (I) $\rightarrow$ Region (R)	High Income (I=1)	$CRY(\theta)$	1.2
Region (R) $\rightarrow$ Gender Bias (G)	Rural (R=0)	$CRY(\theta)$	1.0
Treatment (T) Base Rate	-	$R_Y(\theta)$	0.2
Age (A) $\rightarrow$ Treatment (T)	Old (A=1)	$CRY(\theta)$	1.2
Income (I) $\rightarrow$ Treatment (T)	High Income (I=1)	$CRY(\theta)$	1.0
Gender Bias (G) $\rightarrow$ Treatment (T)	High Bias (G=1)	$CRY(\theta)$ (Negative effect)	1.4
Insurance (S) Base Rate	-	$R_Y(\theta)$	0.3
Treatment (T) $\rightarrow$ Insurance (S)	Treated (T=1)	$CRY(\theta)$	0.8
Age (A) $\rightarrow$ Insurance (S)	Old (A=1)	$CRY(\theta)$	0.4
Hospital (H) Base Rate	-	$R_Y(\theta)$	0.4
Insurance (S) $\rightarrow$ Hospital (H)	Premium (S=1)	$CRY(\theta)$	0.6
Region (R) $\rightarrow$ Hospital (H)	Urban (R=1)	$CRY(\theta)$	0.5
Doctor (D) Base Rate	-	$R_Y(\theta)$	0.5
Hospital (H) $\rightarrow$ Doctor (D)	Advanced (H=1)	$CRY(\theta)$	0.4
Gender Bias (G) $\rightarrow$ Doctor (D)	High Bias (G=1)	$CRY(\theta)$	0.3
Outcome (O) Base Rate	-	$R_Y(\theta)$	0.1
Age (A) $\rightarrow$ Outcome (O)	Young (A=0)	$CRY(\theta)$	0.8
Region (R) $\rightarrow$ Outcome (O)	Rural (R=0)	$CRY(\theta)$	0.6
Treatment (T) $\rightarrow$ Outcome (O)	Treated (T=1)	$CRY(\theta)$	1.2
Doctor (D) $\rightarrow$ Outcome (O)	Senior (D=1)	$CRY(\theta)$	0.5
Hospital (H) $\rightarrow$ Outcome (O)	Advanced (H=1)	$CRY(\theta)$	0.4
Satisfaction (F) Base Rate	-	$R_Y(\theta)$	0.3
Outcome (O) $\rightarrow$ Satisfaction (F)	Good (O=1)	$CRY(\theta)$	0.8
Doctor (D) $\rightarrow$ Satisfaction (F)	Senior (D=1)	$CRY(\theta)$	0.3